

# Driving with DINO: Vision Foundation Features as a Unified Bridge for Sim-to-Real Generation in Autonomous Driving

Xuyang Chen<sup>1,2\*</sup> Conglang Zhang<sup>3,4\*</sup> Chuanheng Fu<sup>3,4\*</sup> Zihao Yang<sup>5</sup> Kaixuan Zhou<sup>3†‡</sup>  
 Yizhi Zhang<sup>3</sup> Jianan He<sup>3</sup> Yanfeng Zhang<sup>2</sup> Mingwei Sun<sup>3,4</sup> Zhen Dong<sup>4</sup>  
 Xiaoxiao Long<sup>6</sup> Zengmao Wang<sup>4‡</sup> Liqiu Meng<sup>1</sup>

<sup>1</sup>Technical University of Munich    <sup>2</sup>Huawei Hilbert Research Center    <sup>3</sup>Huawei Riemann Lab

<sup>4</sup>Wuhan University    <sup>5</sup>University of Science and Technology of China    <sup>6</sup>Nanjing University

\*Equal contribution    †Project lead    ‡Corresponding author



**Figure 1.** Driving with DINO (DwD) achieves photorealistic simulation-to-real video translation with superior structural consistency. As shown, our method generalizes remarkably well across diverse scenarios, ranging from town and urban environments to challenging weather conditions such as rain and frost.

## Abstract

*Driven by the emergence of Controllable Video Diffusion, existing Sim2Real methods for autonomous driving video generation typically rely on explicit intermediate representations to bridge the domain gap. However, these modalities face a fundamental Consistency-Realism Dilemma. Low-level signals (e.g., edges, blurred images) ensure precise control but compromise realism by "baking in" synthetic artifacts, whereas high-level priors (e.g., depth, semantics, HDMaps) facilitate photorealism but lack the struc-*

*tural detail required for consistent guidance. In this work, we present Driving with DINO (DwD), a novel framework that leverages Vision Foundation Module(VFM) features as a unified bridge between the simulation and real-world domains. We first identify that these features encode a spectrum of information, from high-level semantics to fine-grained structure. To effectively utilize this, we employ Principal Subspace Projection to discard the high-frequency elements responsible for 'texture baking,' while concurrently introducing Random Channel Tail Drop to mitigate the structural loss inherent in rigid dimensional-*

ity reduction, thereby reconciling realism with control consistency. Furthermore, to fully leverage DINOv3’s high-resolution capabilities for enhancing control precision, we introduce a learnable Spatial Alignment Module that adapts these high-resolution features to the diffusion backbone. Finally, we propose a Causal Temporal Aggregator employing causal convolutions to explicitly preserve historical motion context when integrating frame-wise DINO features, which effectively mitigates motion blur and guarantees temporal stability. Extensive experiments show that our approach achieves State-of-the-Art performance, significantly outperforming existing baselines in generating photorealistic driving videos that remain faithfully aligned with the simulation.

## 1. Introduction

Closed-loop validation is critical for autonomous driving safety. However, applying it in the real world is risky and inefficient due to the massive data requirements and the scarcity of rare corner cases. Simulation offers a scalable alternative, yet creating photorealistic assets remains costly. Consequently, simulators like CARLA [10] often compromise on visual fidelity, resulting in a significant domain gap between simulated and real-world data. This discrepancy hinders the generalization of simulation-trained models to physical environments, necessitating robust Sim-to-Real transfer techniques to effectively utilize simulation assets.



Figure 2. Consistency-Realism-Dilemma

To address this challenge, Diffusion Models have emerged as a promising paradigm, offering superior stability and high-fidelity generation capabilities. While initial attempts [28, 31] adapted these image diffusion models for Sim-to-Real in a frame-wise manner; however, treating continuous driving video as independent images ignores temporal correlations, inevitably leading to severe flickering artifacts and texture incoherence. To remedy this, leveraging video diffusion models augmented with structural control mechanisms (e.g., ControlNet [53]) emerges as a superior paradigm [16, 17, 23, 27, 43, 47, 55]. Video diffusion inherently model temporal dynamics to ensure coherence, while the integration of ControlNet adapters strictly anchors the generative process to the simulation’s geometric layout. This integration effectively reconciles the tension between

temporal and spatial consistency, making it a highly promising direction for robust Sim-to-Real transfer.

In this context, intermediate representations such as edge maps, blurred images, semantic masks, and depth maps serve as the common bridge between simulation and reality, and have been widely integrated into ControlNet-based frameworks [1, 2, 13, 14]. Additionally, High-Definition Maps (HDMaps) is a widely adopted structural representation in the autonomous driving domain. However, achieving both high photorealism and spatial consistency simultaneously remains a significant challenge, which we call as **Consistency-Realism-Dilemma**. As depicted in Fig. 2, current widely adopted control signals could not balance them well:

- *Low-level signals* (e.g., edges, blurred images) provide strong structural guidance but often impose rigid constraints that “bake in” synthetic textures. This forces the model to retain the simulation’s artificial appearance, hindering the generation of true photorealism.
- *High-level signals* (e.g., depth, semantics, HDMaps) heavily discard structural information to allow for photorealistic generation. However, this lack of fine-grained structural information creates ambiguity, which frequently leads to generative hallucinations and control errors, such as generating spurious or incorrect lane lines.

To leverage the advantages of both feature types, recent multi-control frameworks attempt to mitigate these trade-offs, yet they face significant challenges. Jointly training multiple ControlNets incurs prohibitive GPU memory costs and suffers from gradient conflicts, where heterogeneous modalities compete and fail to converge [7, 18]. Conversely, combining separately trained adapters during inference is equally problematic. Aggregating distinct control signals often leads to feature interference, necessitating laborious weight tuning and frequently resulting in incoherent fusion or visual artifacts due to conflicting guidance [57].

Departing from complex multi-branch designs, we propose a novel conditioning strategy leveraging Vision Foundation Models (VFMs), specifically DINOv3 [37]. Unlike explicit multi-control approaches, DINO features inherently encode a rich spectrum of scene properties ranging from low-level to high-level cues within a unified latent space, a capability validated by its robust performance across a wide spectrum of task granularities [24, 41, 45, 49, 50, 58]. By utilizing DINO as a holistic condition for Sim-to-Real transfer, we achieve a natural fusion of structural and semantic information. Crucially, this approach eliminates the feature competition and gradient conflicts typical of multi-branch architectures, allowing for efficient training and inference without additional computational overhead or complex manual tuning.

Nevertheless, our analysis reveals that naively incorporating DINO features into ControlNet results in textural in-



formation leakage. Since DINO representations are rich enough to serve as powerful encoders for auto-encoding tasks—a property explored in prior work [21, 36, 58]—they inadvertently carry over fine-grained pixel information. In our Sim-to-Real context, the model essentially memorizes and reproduces the synthetic textures of the simulation instead of generating realistic details, thereby defeating the purpose of domain adaptation. Furthermore, the spatial resolution of DINO features is typically down-sampled by a factor of 16. This significant compression results in the loss of critical structural details, particularly along object boundaries, which inevitably degrades control consistency. Conversely, in the temporal domain, DINO features exhibit significant redundancy due to their independent frame-wise processing nature. While existing methods often resort to naive keyframe sampling to mitigate this [4, 35], our analysis suggests that such aggressive subsampling disrupts motion continuity, inevitably leading to temporal aliasing and incoherence in the generated video.

To address these challenges, we propose **Driving with DINO (DwD)**, a controllable video diffusion framework leveraging DINO features to effectively balance visual realism and control consistency through the following contributions:

**Minor Components Pruning.** We reveal that the minor components of VFM features primarily encode high-frequency textural details, which lead to texture baking in Sim-to-Real transfer. Then, we leverage Principal Subspace Projection to attenuate high-frequency details, and introduce *Random Channel Tail Drop* to prevent the significant structural information loss caused by rigid dimensionality reduction. This training strategy stochastically prunes minor components after PCA projection, enabling the model to effectively balance the utilization of semantic and structural information during training, thereby achieving a trade-off between realism and controllability.

**Spatial Resolution Enhancer.** To compensate for the significant spatial information loss of DINO backbones, we leverage DINOv3 to process input videos at higher resolutions. We then introduce a learnable *Spatial Alignment Module* to bridge the consequent dimensionality mismatch with the diffusion backbone, thereby significantly enhancing control consistency.

**Causal Temporal Aggregator.** We introduce the *Causal Temporal Aggregator*, a downsampling module driven by causal convolutions. It addresses temporal redundancy by preserving historical context, effectively mitigating motion blur and enhancing stability.

## 2. Related Works

### 2.1. Generative Adversarial Networks

Early Sim-to-Real approaches utilized GANs (e.g., CycleGAN [59], CUT [30]) to align simulated images with real-world distributions. However, these adversarial translations frequently introduce geometric distortions and semantic inconsistencies. While utilizing simulator-derived G-buffers (e.g., depth, normals) can constrain the generation process to preserve geometry [34], such methods often retain adversarial artifacts and lack fine-grained texture fidelity.

### 2.2. 2D Image and Video Diffusion

Diffusion models have mitigated GAN-based instability through superior fine-grained fidelity. SDEdit [28] facilitates transfer via SDE inversion [38], injecting photorealistic priors while maintaining the simulator’s semantic structure. Extensions to video (e.g., Pix2Video [6], TokenFlow [15]) enforce temporal coherence within zero-shot frameworks by propagating features or injecting optical flow priors (FLATTEN [9]).

However, methods relying on inversion or diffusion-based relighting [25, 54] struggle to effectively disentangle semantic structure from synthetic style, resulting in severe “texture baking.” To address this, ControlNet [53] introduced explicit spatial conditioning to decouple geometry from appearance. With the rise of Video Diffusion Transformers (DiTs) [32], controllable generation has shifted towards inherently modeling motion dynamics, offering temporal consistency superior to zero-shot adaptations.

### 2.3. Controllable Video Diffusion

In autonomous driving simulation, methods like MagicDrive [13, 14] and DriveDreamer [44, 56] utilize sparse high-level priors (e.g., HDMaps, 3D boxes). While effective for layout, the spatial sparsity of these signals leads to hallucinations in unconstrained regions. Conversely, volumetric approaches like WoVoGen [26] utilize 3D occupancy for consistency but remain too coarse-grained for fine geometric details.

Recent efforts to unify these paradigms, such as Cosmos Transfer [1, 2], incorporate both high-level semantic and low-level geometric cues. However, fusing such heterogeneous signals introduces significant architectural complexity and instability, often hitting a *Consistency-Realism Dilemma*. Existing multi-control fusion strategies are either limited to similar modalities [12] or suffer from prohibitive training costs [48]. To address these limitations, we propose utilizing DINOv3 as a unified representation that encapsulates both semantics and structures, allowing it to be seamlessly integrated into a standard single-control architecture. While DINO has been applied to object-level control [8, 22], we extend this to scene-level Sim-to-Real trans-

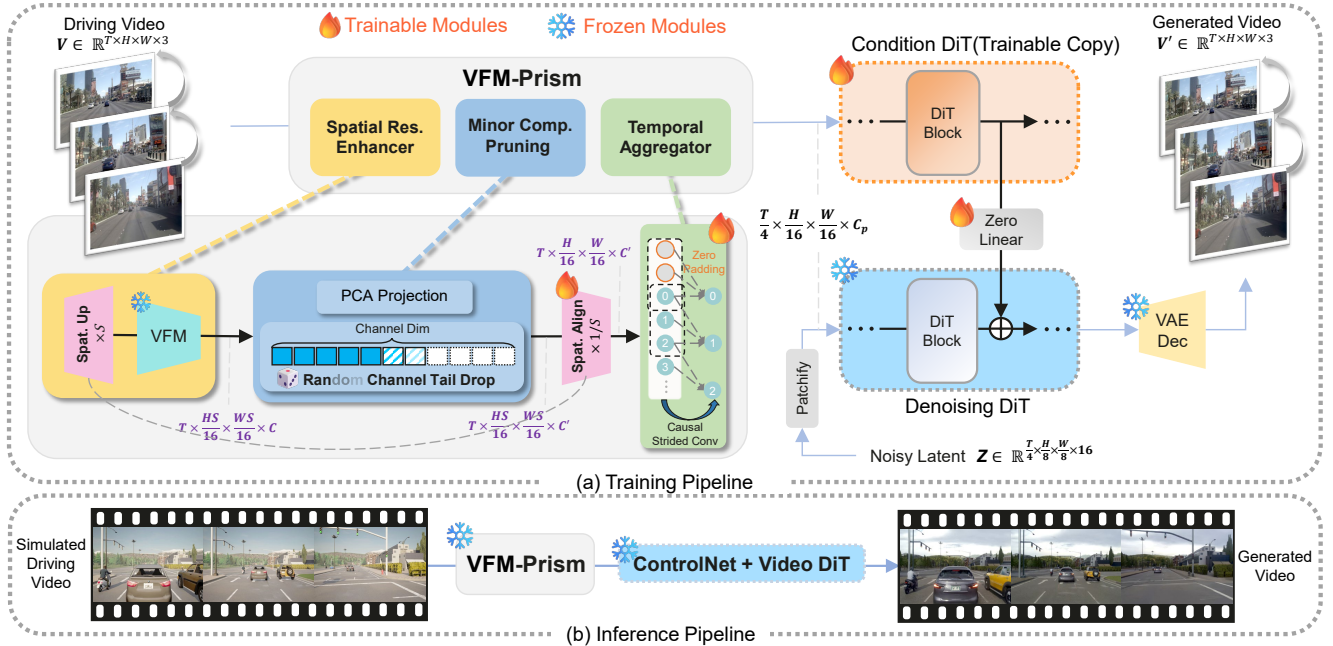


Figure 3. The framework of Dwd. (a) Training: The model is trained on real-world driving videos using a controllable diffusion architecture. The core module, VFM-Prism, processes DINOv3 features through Spatial Resolution Enhancement, Minor Components Pruning, and Causal Temporal Aggregation. These refined features are injected via a Control Branch to guide the reconstruction of the original video. (b) Inference: The model performs Sim-to-Real translation using synthetic inputs. By leveraging the domain-invariant structural features extracted by VFM-Prism (specifically via PCA-based pruning to mitigate texture leakage), Dwd generates high-fidelity photorealistic videos that strictly preserve the simulation’s geometric layout.

fer, utilizing a unified representation to reconcile photorealism with strict structural consistency and eliminate texture baking.

### 3. Method

#### 3.1. Overview

Dwd is a diffusion-based framework designed to translate synthetic driving simulations into photorealistic video sequences. At its core, the framework leverages Vision Foundation Model (VFM) latents as an intermediate semantic bridge. The methodology is organized as follows: Sec. 3.2 details the backbone video diffusion architecture. Sec. 3.3 introduces *VFM-Prism*, a feature processing module tailored to ensure robust Sim2Real alignment during training. Finally, Sec. 3.4 delineates the inference pipeline used to transform synthetic inputs into realistic videos.

#### 3.2. Controllable Video Diffusion Model

The Dwd framework leverages the architecture of the pretrained Cosmos-Predict2.5 [2], which integrates the WAN2.1 3D VAE [40] with fine-tuned Diffusion Transformer (DiT) blocks. To enable structurally controllable generation, we augment the video diffusion framework with a dedicated control branch, as illustrated in Fig. 3(a). This

branch comprises conditioning DiT blocks initialized with weights from the denoising DiT backbone. Following the injection strategy proposed in VACE [23], control features are modulated into the base model at uniform intervals of  $N$  blocks. The control branch encodes processed DINOv3 latents as conditioning inputs. During the training phase, the model is optimized to reconstruct ground-truth realistic videos. At inference (Fig. 3(b)), the model processes synthetic simulation inputs to generate photorealistic counterparts, effectively bridging the domain gap between simulation and reality.

#### 3.3. Robust Training with VFM-Prism

To integrate VFM features into Sim2Real translation, we propose a module named *VFM-Prism* to mitigate the aforementioned challenges—specifically the high spatial compression of DINOv3, textural leakage, and the latent dimensionality mismatch with DiT blocks. As illustrated in Fig. 3(a), the pipeline comprises three core modules: *Spatial Resolution Enhancer*, *Minor Components Pruning*, and *Causal Temporal Aggregator*, each detailed in the following sections.

**Spatial Resolution Enhancer.** Unlike previous VFMs [29, 33, 39] that exhibit bias against high-resolution inputs, DINOv3 demonstrates robustness to variable reso-

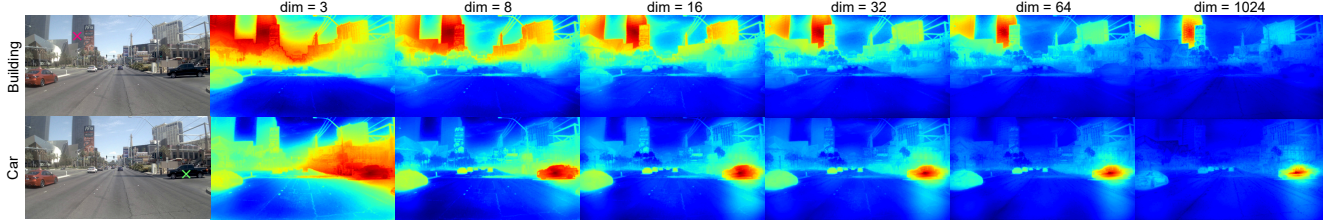


Figure 4. Lower-dimensional PCA components encode coarse semantic layouts, whereas increasing the dimensions leads to the refinement of high-frequency details. Similarity maps are shown for two anchor points (top:  $\times$  on building, bottom:  $\times$  on one car).

lutions due to its specialized positional encoding strategy (RoPE-box jittering). To compensate for the high spatial compression rate of DINOv3, we upsample the input video  $V \in \mathbb{R}^{T \times H \times W \times 3}$  by a scale factor  $S$  prior to encoding, yielding a higher-resolution feature map  $Z_c \in \mathbb{R}^{T \times \frac{H \times S}{16} \times \frac{W \times S}{16} \times C}$ . While post-hoc feature map upsampling methods like Featup [11] and Anyup [46] offer computationally cheaper alternatives, our empirical findings suggest they compromise feature map quality, negatively impacting the consistency between generated videos and input simulations. Thus, input-space upscaling ensures superior structural fidelity. However, this results in a latent tensor size misaligned with the input requirements of the Condition DiT blocks, which should spatially be  $\frac{H}{16} \times \frac{W}{16}$  rather than  $\frac{H \times S}{16} \times \frac{W \times S}{16}$ . Therefore, we introduce a **Spatial Alignment Module** to bridge this gap, which is composed of strided convolutions with residual blocks, as detailed in the Appendix.

**Minor Components Pruning.** To mitigate texture leakage and extract domain-invariant structural conditions, we employ Principal Component Analysis (PCA) to construct a semantic bottleneck. By projecting the high-dimensional feature space onto a lower-dimensional subspace  $\mathbb{R}^k$ , we effectively filter out low-variance components associated with appearance while retaining dominant structural information. Qualitative analysis of feature similarity (Fig. 4) indicates that the dimensionality  $k$  acts as a critical hyperparameter for this disentanglement. Extremely low dimensions (e.g.,  $k = 3$ ) compromise spatial granularity, causing semantic ambiguity. Conversely, a high-dimensional spectrum (e.g.,  $k = 64$ ) retains excessive high-frequency information, resulting in similarity hotspots driven by local texture rather than geometry—indicative of domain noise leakage. We observe that a moderate subspace (e.g.,  $k \in \{8, 16, 32\}$ ) strikes an optimal balance, preserving structural layout while suppressing domain-specific texture.

Although the leading PCA components primarily encode semantics, a distinct boundary between structure and style is ill-defined. To prevent the loss of structural information associated with rigid dimensionality reduction, we propose *Random Channel Tail Drop*, a stochastic regularization strategy. During training, rather than using a fixed

truncation point, we sample the number of active channels  $k$  from a predefined discrete set of candidate dimensions  $\mathcal{K} = \{k_1, k_2, \dots, k_m\}$ . We then apply a channel-wise binary mask  $M \in \{0, 1\}^{k_m}$  with entries  $M_i = 1$  if  $i \leq k$  and 0 otherwise.

**Causal Temporal Aggregator.** The absence of temporal compression in DINOv3, results in a temporal dimension misalignment with the input requirements of the Condition DiT blocks. While prior methods rely on heuristic down-sampling strategies such as keyframe sampling [4, 20] or bilinear interpolation [35], these approaches often fail to capture fine-grained spatial details and temporal dynamics. To bridge this gap without incurring the computational overhead of a full CausalVAE, we insert extra causal convolution blocks into aforementioned Spatial Alignment Module (see Appendix).

### 3.4. Video Sim2Real Translation

Once trained, DwD is employed to perform Video Sim2Real Translation. As illustrated in Fig. 3(b), the inference process takes a synthetic video rendered from a driving simulator as input. While the pipeline largely mirrors the training phase, we introduce a key flexibility during inference: we manually modulate the number  $k$  of active PCA components (i.e., the spectral truncation threshold). This adjustment allows us to explicitly control the guidance strength, effectively balancing structural fidelity with realistic texture generation.

## 4. Experiments

### 4.1. Experiment Setup

We train DwD on the nuPlan dataset [5] and evaluate performance using videos rendered from the CARLA simulator (see Appendix for more details). To ensure a comprehensive assessment, we compare our method against representative baselines across different categories. For training-free image diffusion models like TC-Light [25], we adhere to the official protocols using appropriate relighting prompts. For FRESKO [51], we additionally incorporate nuPlan images as reference style inputs. In the video generation domain, we compare against Cosmos-Transfer2.5 [2] with various



input modalities. Crucially, to ensure a fair comparison, we fine-tune the ControlNet modules of these video generation baselines on the same training set used for our method.

## 4.2. Evaluation Metrics.

Sim-to-Real video translation must balance consistency and realism. To provide a comprehensive evaluation, we assess the results along the following three dimensions:

- *Visual Fidelity*: We employ **sFID** and **sKID** to measure distribution discrepancy, adopting a semantics-aware sampling strategy [34] to mitigate layout mismatches. By matching VGG features between CG and real patches, we construct a benchmark of 400,000 pairs for robust evaluation.
- *Perceptual Realism*: We quantify authenticity via **CLIP-Real** [52], formulated as  $\text{CLIP-Real} = (x^\top t_p)/(x^\top t_n)$ . Here,  $x, t_p, t_n$  represent embeddings of the output frame, positive (e.g., “Photo”), and negative (e.g., “Game”) prompts, respectively. Higher scores indicate better alignment with real photography.
- *Temporal Consistency*: We assess temporal coherence using **Motion-S** [19] for motion plausibility and **WarpSSIM**. The latter computes SSIM between a frame and its neighbors warped via optical flow derived from source CG videos.
- *Sim2Real Consistency*: We assess semantic preservation using the mean Intersection over Union (**mIoU**). Specifically, we employ the state-of-the-art perception model [42] (pretrained on Cityscapes) to perform semantic segmentation on the translated frames. We then calculate the mIoU by comparing the predicted segmentation masks against the ground truth semantic labels derived from the source CG engine.

## 4.3. Quantitative Evaluation.

Tab. 1 highlights DwD’s substantial advantage in fidelity metrics (sKID and sFID). As previously analyzed, low-level conditions (e.g., edge, blur) exhibit poor fidelity primarily due to their CG-like textures, which significantly deviate from real-world data distributions. Counter-intuitively, high-level modalities like segmentation and depth also fail to achieve competitive sFID/sKID scores. This stems from their insufficient control capability, which leads to pronounced layout discrepancies between the generated content and the ground truth. Since sFID and sKID are computed based on aligned spatial regions, such structural misalignments inevitably penalize the fidelity scores. In contrast, DwD effectively bridges this gap by balancing precise layout guidance with high-quality synthesis, resulting in superior performance.

In terms of photorealism (measured by CLIP-Real), DwD achieves performance comparable to methods utilizing high-level structural conditions, such as depth and

semantic maps. In contrast, low-level conditions tend to produce textures that closely mirror the original synthetic videos (CG), resulting in a CLIP-Real score (100.63 for blur and 112.38 for edge) similar to that of the CG baseline (98.79). TC-Light exhibits a similar trend (102.46) as it primarily modifies environment lighting without altering underlying textures.

Regarding temporal consistency, DwD demonstrates superior performance on the Motion-S metric. In terms of WarpSSIM, DwD is only slightly below Edge-based methods while outperforming Seg- and Depth-based approaches. Notably, TC-Light achieves an outlier WarpSSIM score by nearly identical preservation of original CG textures; however, this comes at a severe expense of realism.

Table 3 reports the Sim2Real consistency reflected by mIoU. Our method exhibits high mIoU scores across multiple categories, demonstrating consistency comparable to robust low-level control signals such as Edge and Blur. Furthermore, a comparison with the low-resolution alternative verifies that spatial resolution enhancement significantly contributes to structural consistency.

Table 1. Quantitative evaluations. Top results are colored in Gold, Silver, and Bronze (also applicable to Tabs. 2 and 3). † denotes modules fine-tuned on the same dataset as DwD. C-T2.5 stands for Cosmos-Transfer 2.5.

Method	Mot-S <sup>†</sup> (%)	W-SSIM <sup>†</sup>	CLIP-R <sup>†</sup>	sKID <sup>↓</sup>	sFID <sup>↓</sup>
CG	-	-	98.79	29.59	43.65
FRESCO	98.37	93.32	109.92	32.55	56.28
TC-Light	98.79	96.59	102.46	22.12	44.47
C-T2.5 Edge	98.61	93.60	112.38	22.82	37.44
C-T2.5 Edge <sup>†</sup>	98.73	94.37	112.58	21.22	32.59
C-T2.5 Blur	98.02	88.14	100.63	29.09	39.57
C-T2.5 Depth	98.47	92.48	116.50	26.98	38.44
C-T2.5 Edge+Depth	93.97	93.97	112.15	23.71	36.69
C-T2.5 Edge+Seg	98.62	93.97	112.13	23.32	36.62
C-T2.5 Seg	98.85	90.92	119.73	23.81	37.20
<b>Ours</b>	98.94	93.07	119.11	9.30	21.62

## 4.4. Qualitative Evaluation.

We conduct a qualitative comparison between the photorealistic videos generated by DwD and baseline methods. As illustrated in Fig. 5, DwD not only ensures semantic consistency but also maintains precise control over structural details, particularly for road lines and markings. This effectively addresses the challenge of balancing low-level and high-level control signals discussed in the Introduction.

Specifically, high-level signals (e.g., depth or semantic maps) often cause hallucinations in background regions. While semantic maps can produce accurate lane markings when guided by explicit instance segmentation, they tend to hallucinate non-existent lines when the input lacks such





Figure 5. **Qualitative comparison with state-of-the-art methods.** The **red boxes** highlight **inconsistencies** with respect to the CG input, while the **green boxes** point out **low-fidelity textures**.



markings (see Fig. 12 and Fig. 13). Conversely, low-level control signals tend to yield oversimplified outputs that adhere too closely to the synthetic domain. For instance, Cosmos-T2.5 Blur merely reproduces the synthetic input. Similarly, Cosmos-T2.5 Edge lacks realism because the edges extracted from CG are excessively clean and regular, thereby inherently carrying texture information from the CG source that biases the generation toward a synthetic appearance. Although the multi-control variant, Cosmos-T2.5 Edge+Depth, attempts to strike a balance, its performance remains inferior to DwD.

#### 4.5. Ablation Studies

We systematically evaluate the impact of key hyperparameters and components in Tab. 2. First, we investigate the influence of the active PCA channels  $k$  during inference. We observe that fidelity metrics gradually improve as  $k$  decreases; we attribute this to high-level texture leakage caused by insufficient pruning of PCA-projected features. However, excessive pruning (e.g.,  $k = 3$ ) causes fidelity to degenerate, as the model struggles to maintain semantic consistency—a limitation shared with Cosmos T2.5 Seg. Given these findings, we select  $k = 8$  as our optimal dimensionality for inference, as it strikes the best balance between preserving structural guidance and ensuring generative realism.

Subsequently, we analyze the influence of the feature upscaling factor  $S$ . While a factor of  $\times 4$  leads to a slight decrease in sFID and sKID, it yields a substantial improvement in temporal consistency (W-SSIM). As illustrated in the Appendix, higher  $S$  indeed leads to better structural consistency, which should be beneficial to sFID and sKID. We attribute the subsequent decrease in fidelity metrics to the domain gap in sharpness: the generated videos preserve the pristine edges of the source CG, which statistically diverges from the inherent motion blur and noise found in real video. Finally, we verify the efficacy of the Causal Temporal Aggregator. Compared to the  $\times 4$  baseline, this component simultaneously enhances Warp-SSIM and improves fidelity metrics (sFID, sKID). This performance gain is primarily attributed to the aggregator’s ability to mitigate blur and corrupted frames in the generated videos, which significantly elevates overall generative quality. Furthermore, the mIoU scores in Tab. 3 provide additional evidence that both the Spatial Resolution Enhancer and the Causal Temporal Aggregator substantially boost controllability. To offer a more intuitive perspective that quantitative metrics may obscure, we provide additional visual comparisons in the appendix, clearly illustrating the distinct effects of varying hyperparameters.

Table 2. Ablation studies.  $\times S$  means the upscaling spatial resolution  $S$  times.

Method	W-SSIM $\uparrow$	CLIP-R $\uparrow$	sKID $\downarrow$	sFID $\downarrow$
pca3 ( $\times 1$ )	90.94	119.63	10.70	23.32
pca8 ( $\times 1$ )	91.34	118.78	9.08	21.37
pca16 ( $\times 1$ )	91.49	116.00	9.92	22.60
pca32 ( $\times 1$ )	90.29	114.38	9.91	23.01
pca8 ( $\times 2$ )	90.73	118.38	9.79	23.06
pca8 ( $\times 4$ )	92.69	118.89	9.68	21.92
pca8 ( $\times 4$ )+Temp (final)	93.07	119.11	9.30	21.62

Table 3. Comparison of mIoU across different methods and categories.

Category	pca8 ( $\times 1$ )	Edge	Blur	Depth	Seg	Ours
Road	0.9574	0.9591	0.9636	0.9475	0.9345	0.9605
Sidewalk	0.5464	0.5914	0.6332	0.5253	0.5010	0.5610
Building	0.7802	0.8193	0.8127	0.7725	0.5781	0.8087
Fence	0.0978	0.0767	0.0790	0.0789	0.0848	0.1187
Pole	0.2757	0.3665	0.3214	0.3548	0.2555	0.3435
Traffic Light	0.4354	0.6655	0.5501	0.5392	0.3174	0.4503
Traffic Sign	0.2014	0.3838	0.2862	0.2601	0.1505	0.2681
Vegetation	0.6907	0.6833	0.7210	0.6936	0.5773	0.7150
Terrain	0.3171	0.3561	0.4476	0.3284	0.3210	0.3245
Sky	0.8945	0.8912	0.9028	0.9115	0.7691	0.9111
Person	0.5380	0.6795	0.6729	0.6438	0.5828	0.6256
Car	0.7522	0.7973	0.7819	0.7828	0.7044	0.7756
Bus	0.0989	0.0223	0.0620	0.0259	0.0049	0.0296
Bicycle	0.0599	0.0242	0.0132	0.0294	0.0612	0.0666
<b>mIoU (Avg)</b>	0.4675	0.5015	0.5105	0.4843	0.4132	0.4967

## 5. Conclusion

In this paper, we propose Driving with DINO (DwD), which leverages Vision Foundation Models to resolve the “Consistency-Realism-Dilemma” in Sim-to-Real video translation. By comparing DwD with state-of-the-art baselines on diverse simulated datasets and our self-collected data, we verify the significant advantages of DwD in achieving superior visual realism and structural consistency. While our results are promising, we acknowledge that computational constraints currently limit the exploration of the model’s full capacity. Accordingly, future work will focus on validating the scalability of our approach on large-scale, high-resolution driving datasets and investigating its deployment within closed-loop autonomous driving systems.

## References

- [1] Hassan Abu Alhaja, Jose Alvarez, Maciej Bala, Tiffany Cai, Tianshi Cao, Liz Cha, Joshua Chen, Mike Chen, Francesco Ferroni, Sanja Fidler, et al. Cosmos-transfer1: Conditional world generation with adaptive multimodal control. *arXiv preprint arXiv:2503.14492*, 2025. 2, 3
- [2] Arslan Ali, Junjie Bai, Maciej Bala, Yogesh Balaji, Aaron Blakeman, Tiffany Cai, Jiaxin Cao, Tianshi Cao, Eliza-



- beth Cha, Yu-Wei Chao, et al. World simulation with video foundation models for physical ai. *arXiv preprint arXiv:2511.00062*, 2025. 2, 3, 4, 5
- [3] Shuai Bai, Yuxuan Cai, Ruizhe Chen, Keqin Chen, Xionghui Chen, Zesen Cheng, Lianghao Deng, Wei Ding, Chang Gao, Chunjiang Ge, Wenbin Ge, Zhifang Guo, Qidong Huang, Jie Huang, Fei Huang, Binyuan Hui, Shutong Jiang, Zhao-hai Li, Mingsheng Li, Mei Li, Kaixin Li, Zicheng Lin, Junyang Lin, Xuejing Liu, Jiawei Liu, Chenglong Liu, Yang Liu, Dayiheng Liu, Shixuan Liu, Dunjie Lu, Ruilin Luo, Chenxu Lv, Rui Men, Lingchen Meng, Xuancheng Ren, Xingzhang Ren, Sibao Song, Yuchong Sun, Jun Tang, Jianhong Tu, Jianqiang Wan, Peng Wang, Pengfei Wang, Qiuyue Wang, Yuxuan Wang, Tianbao Xie, Yiheng Xu, Haiyang Xu, Jin Xu, Zhibo Yang, Mingkun Yang, Jianxin Yang, An Yang, Bowen Yu, Fei Zhang, Hang Zhang, Xi Zhang, Bo Zheng, Humen Zhong, Jingren Zhou, Fan Zhou, Jing Zhou, Yuanzhi Zhu, and Ke Zhu. Qwen3-vl technical report. *arXiv preprint arXiv:2511.21631*, 2025. 12
- [4] Ryan Burgert, Yuancheng Xu, Wenqi Xian, Oliver Pilarski, Pascal Clausen, Mingming He, Li Ma, Yitong Deng, Lingxiao Li, Mohsen Mousavi, et al. Go-with-the-flow: Motion-controllable video diffusion models using real-time warped noise. In *Proceedings of the Computer Vision and Pattern Recognition Conference*, pages 13–23, 2025. 3, 5
- [5] Holger Caesar, Juraj Kabzan, Kok Seang Tan, Whye Kit Fong, Eric Wolff, Alex Lang, Luke Fletcher, Oscar Beijbom, and Sammy Omari. nuplan: A closed-loop ml-based planning benchmark for autonomous vehicles. *arXiv preprint arXiv:2106.11810*, 2021. 5, 12
- [6] Duygu Ceylan, Chun-Hao P Huang, and Niloy J Mitra. Pix2video: Video editing using image diffusion. In *Proceedings of the IEEE/CVF International Conference on Computer Vision*, pages 23206–23217, 2023. 3
- [7] Weifeng Chen, Jie Wu, Pan Pan, Wanyi Xing, Yi Lu, Zhou Li, and Gang Zhao. Control-a-video: Controllable text-to-video generation with diffusion models. *arXiv preprint arXiv:2305.13840*, 2023. 2
- [8] Xi Chen, Lianghua Huang, Yu Liu, Yujun Shen, Deli Zhao, and Heng-Guan Heng. Anydoor: Zero-shot object-level image customization. In *CVPR*, 2024. 3
- [9] Yuren Cong, Mengmeng Xu, Christian Simon, Shoufa Chen, Jiawei Ren, Yanping Xie, Juan-Manuel Perez-Rua, Bodo Rosenhahn, Tao Xiang, and Sen He. Flatten: optical flow-guided attention for consistent text-to-video editing. *arXiv preprint arXiv:2310.05922*, 2023. 3
- [10] Alexey Dosovitskiy, German Ros, Felipe Codevilla, Antonio Lopez, and Vladlen Koltun. Carla: An open urban driving simulator. In *Conference on robot learning*, pages 1–16. PMLR, 2017. 2
- [11] Stephanie Fu, Mark Hamilton, Laura Brandt, Axel Feldman, Zhoutong Zhang, and William T Freeman. Featup: A model-agnostic framework for features at any resolution. *arXiv preprint arXiv:2403.10516*, 2024. 5
- [12] J. Gao, Z. Chen, X. Liu, J. Feng, C. Si, Y. Fu, et al. Longvie: Multimodal-guided controllable ultra-long video generation. *arXiv preprint arXiv:2508.03694*, 2025. 3
- [13] Ruiyuan Gao, Kai Chen, Enze Xie, Lanqing Hong, Zhenguo Li, Dit-Yan Yeung, and Qiang Xu. Magicdrive: Street view generation with diverse 3d geometry control. *arXiv preprint arXiv:2310.02601*, 2023. 2, 3
- [14] Ruiyuan Gao, Kai Chen, Bo Xiao, Lanqing Hong, Zhenguo Li, and Qiang Xu. Magicdrive-v2: High-resolution long video generation for autonomous driving with adaptive control. In *Proceedings of the IEEE/CVF International Conference on Computer Vision*, pages 28135–28144, 2025. 2, 3
- [15] Michal Geyer, Omer Bar-Tal, Shai Bagon, and Tali Dekel. Tokenflow: Consistent diffusion features for consistent video editing. *arXiv preprint arXiv:2307.10373*, 2023. 3
- [16] Yuwei Guo, Ceyuan Yang, Anyi Rao, Maneesh Agrawala, Dahua Lin, and Bo Dai. Sparsectrl: Adding sparse controls to text-to-video diffusion models. In *European Conference on Computer Vision*, pages 330–348. Springer, 2024. 2
- [17] Hao He, Yinghao Xu, Yuwei Guo, Gordon Wetzstein, Bo Dai, Hongsheng Li, and Ceyuan Yang. Cameractrl: Enabling camera control for text-to-video generation. *arXiv preprint arXiv:2404.02101*, 2024. 2
- [18] Zhihao Hu and Dong Xu. Videocontrolnet: A motion-guided video-to-video translation framework by using diffusion model with controlnet. In *Proceedings of the 31st ACM International Conference on Multimedia*, pages 6467–6476, 2023. 2
- [19] Ziqi Huang, Yinan He, Jiashuo Yu, Fan Zhang, Chenyang Si, Yuming Jiang, Yuanhan Zhang, Tianxing Wu, Qingyang Jin, Nattapol Chanpaisit, et al. Vbench: Comprehensive benchmark suite for video generative models. In *Proceedings of the IEEE/CVF Conference on Computer Vision and Pattern Recognition*, pages 21807–21818, 2024. 6
- [20] Sungwon Hwang, Hyojin Jang, Kinam Kim, Minho Park, and Jaegul Choo. Cross-frame representation alignment for fine-tuning video diffusion models. *arXiv preprint arXiv:2506.09229*, 2025. 5
- [21] Mingkai Jia, Mingxiao Li, Liaoyuan Fan, Tianxing Shi, Jiaxin Guo, Zeming Li, Xiaoyang Guo, Xiao-Xiao Long, Qian Zhang, Ping Tan, et al. Dino-tok: Adapting dino for visual tokenizers. *arXiv preprint arXiv:2511.20565*, 2025. 3
- [22] J. Jiang, G. Hong, M. Zhang, H. Hu, K. Zhan, R. Shao, and L. Nie. Dive: Efficient multi-view driving scenes generation based on video diffusion transformer. *arXiv preprint arXiv:2504.19614*, 2025. 3
- [23] Zeyinzi Jiang, Zhen Han, Chaojie Mao, Jingfeng Zhang, Yulin Pan, and Yu Liu. Vace: All-in-one video creation and editing. *arXiv preprint arXiv:2503.07598*, 2025. 2, 4
- [24] Alexander Kirillov, Eric Mintun, Nikhila Ravi, Hanzi Mao, Chloe Rolland, Laura Gustafson, Tete Xiao, Spencer Whitehead, Alexander C Berg, Wan-Yen Lo, et al. Segment anything. In *Proceedings of the IEEE/CVF international conference on computer vision*, pages 4015–4026, 2023. 2
- [25] Yang Liu, Chuanchen Luo, Zimo Tang, Yingyan Li, Yuanyong Ning, Lue Fan, Junran Peng, Zhaoxiang Zhang, et al. Tc-light: Temporally coherent generative rendering for realistic world transfer. In *The Thirty-ninth Annual Conference on Neural Information Processing Systems*, 2025. 3, 5

- [26] Jiachen Lu, Ze Huang, Zeyu Yang, Jiahui Zhang, and Li Zhang. Wovogen: World volume-aware diffusion for controllable multi-camera driving scene generation. In *European Conference on Computer Vision*, pages 329–345. Springer, 2024. 3
- [27] Wan-Duo Kurt Ma, John P Lewis, and W Bastiaan Kleijn. Trailblazer: Trajectory control for diffusion-based video generation. In *SIGGRAPH Asia 2024 Conference Papers*, pages 1–11, 2024. 2
- [28] Chenlin Meng, Yutong He, Yang Song, Jiaming Song, Junjun Wu, Jun-Yan Zhu, and Stefano Ermon. Sedit: Guided image synthesis and editing with stochastic differential equations. *arXiv preprint arXiv:2108.01073*, 2021. 2, 3
- [29] Maxime Oquab, Timothée Darcet, Théo Moutakanni, Huy Vo, Marc Szafraniec, Vasil Khalidov, Pierre Fernandez, Daniel Haziza, Francisco Massa, Alaaeldin El-Nouby, et al. Dinov2: Learning robust visual features without supervision. *arXiv preprint arXiv:2304.07193*, 2023. 4
- [30] Taesung Park, Alexei A Efros, Richard Zhang, and Jun-Yan Zhu. Contrastive learning for unpaired image-to-image translation. In *Computer Vision—ECCV 2020: 16th European Conference, Glasgow, UK, August 23–28, 2020, Proceedings, Part IX 16*, pages 319–345. Springer, 2020. 3
- [31] Gaurav Parmar, Taesung Park, Srinivasa Narasimhan, and Jun-Yan Zhu. One-step image translation with text-to-image models. *arXiv preprint arXiv:2403.12036*, 2024. 2
- [32] William Peebles and Saining Xie. Scalable diffusion models with transformers. In *Proceedings of the IEEE/CVF International Conference on Computer Vision (ICCV)*, pages 4195–4205, 2023. 3
- [33] Alec Radford, Jong Wook Kim, Chris Hallacy, Aditya Ramesh, Gabriel Goh, Sandhini Agarwal, Girish Sastry, Amanda Askell, Pamela Mishkin, Jack Clark, et al. Learning transferable visual models from natural language supervision. In *International conference on machine learning*, pages 8748–8763. PmlR, 2021. 4
- [34] Stephan R Richter, Hassan Abu AlHaija, and Vladlen Koltun. Enhancing photorealism enhancement. *IEEE Transactions on Pattern Analysis and Machine Intelligence*, 45(2): 1700–1715, 2022. 3, 6
- [35] Lloyd Russell, Anthony Hu, Lorenzo Bertoni, George Fedoseev, Jamie Shotton, Elahe Arani, and Gianluca Corrado. Gaia-2: A controllable multi-view generative world model for autonomous driving. *arXiv preprint arXiv:2503.20523*, 2025. 3, 5
- [36] Minglei Shi, Haolin Wang, Wenzhao Zheng, Ziyang Yuan, Xiaoshi Wu, Xintao Wang, Pengfei Wan, Jie Zhou, and Jiwen Lu. Latent diffusion model without variational autoencoder. *arXiv preprint arXiv:2510.15301*, 2025. 3
- [37] Oriane Siméoni, Huy V Vo, Maximilian Seitzer, Federico Baldassarre, Maxime Oquab, Cijo Jose, Vasil Khalidov, Marc Szafraniec, Seungeun Yi, Michaël Ramamonjisoa, et al. Dinov3. *arXiv preprint arXiv:2508.10104*, 2025. 2
- [38] Jiaming Song, Chenlin Meng, and Stefano Ermon. Denoising diffusion implicit models. *arXiv preprint arXiv:2010.02502*, 2020. 3
- [39] Michael Tschanen, Alexey Gritsenko, Xiao Wang, Muhammad Ferjad Naem, Ibrahim Alabdulmohsin, Nikhil Parthasarathy, Talfan Evans, Lucas Beyer, Ye Xia, Basil Mustafa, et al. Siglip 2: Multilingual vision-language encoders with improved semantic understanding, localization, and dense features. *arXiv preprint arXiv:2502.14786*, 2025. 4
- [40] Team Wan, Ang Wang, Baole Ai, Bin Wen, Chaojie Mao, Chen-Wei Xie, Di Chen, Feiwu Yu, Haiming Zhao, Jianxiao Yang, et al. Wan: Open and advanced large-scale video generative models. *arXiv preprint arXiv:2503.20314*, 2025. 4
- [41] Jianyuan Wang, Minghao Chen, Nikita Karaev, Andrea Vedaldi, Christian Rupprecht, and David Novotny. Vgg: Visual geometry grounded transformer. In *Proceedings of the Computer Vision and Pattern Recognition Conference*, pages 5294–5306, 2025. 2
- [42] Wenhai Wang, Jifeng Dai, Zhe Chen, Zhenhang Huang, Zhiqi Li, Xizhou Zhu, Xiaowei Hu, Tong Lu, Lewei Lu, Hongsheng Li, et al. Internimage: Exploring large-scale vision foundation models with deformable convolutions. In *Proceedings of the IEEE/CVF conference on computer vision and pattern recognition*, pages 14408–14419, 2023. 6
- [43] Xiang Wang, Hangjie Yuan, Shiwei Zhang, Dayou Chen, Jiniu Wang, Yingya Zhang, Yujun Shen, Deli Zhao, and Jingren Zhou. Videocomposer: Compositional video synthesis with motion controllability. *Advances in Neural Information Processing Systems*, 36:7594–7611, 2023. 2
- [44] Xiaofeng Wang, Zheng Zhu, Guan Huang, Xinze Chen, Jiayang Zhu, and Jiwen Lu. Drivedreamer: Towards real-world-drive world models for autonomous driving. In *European conference on computer vision*, pages 55–72. Springer, 2024. 3
- [45] Yifan Wang, Jianjun Zhou, Haoyi Zhu, Wenzheng Chang, Yang Zhou, Zizun Li, Junyi Chen, Jiangmiao Pang, Chunhua Shen, and Tong He.  $\pi^3$ : Permutation-equivariant visual geometry learning. *arXiv preprint arXiv:2507.13347*, 2025. 2
- [46] Thomas Wimmer, Prune Truong, Marie-Julie Rakotosaona, Michael Oechsle, Federico Tombari, Bernt Schiele, and Jan Eric Lenssen. Anyup: Universal feature upsampling. *arXiv preprint arXiv:2510.12764*, 2025. 5, 13
- [47] Dianbing Xi, Jiepeng Wang, Yuanzhi Liang, Xi Qiu, Yuchi Huo, Rui Wang, Chi Zhang, and Xuelong Li. Omnividiff: Omni controllable video diffusion for generation and understanding. *arXiv preprint arXiv:2504.10825*, 2025. 2
- [48] D. Xi, J. Wang, Y. Liang, X. Qiu, J. Liu, H. Pan, et al. Ctrlviddiff: Controllable video generation via unified multimodal video diffusion. *arXiv preprint arXiv:2511.21129*, 2025. 3
- [49] Gangwei Xu, Haotong Lin, Hongcheng Luo, Xianqi Wang, Jingfeng Yao, Lianghui Zhu, Yuechuan Pu, Cheng Chi, Haiyang Sun, Bing Wang, et al. Pixel-perfect depth with semantics-prompted diffusion transformers. *arXiv preprint arXiv:2510.07316*, 2025. 2
- [50] Lihe Yang, Bingyi Kang, Zilong Huang, Xiaogang Xu, Jiashi Feng, and Hengshuang Zhao. Depth anything: Unleashing the power of large-scale unlabeled data. In *Proceedings of the IEEE/CVF conference on computer vision and pattern recognition*, pages 10371–10381, 2024. 2

- [51] Shuai Yang, Yifan Zhou, Ziwei Liu, and Chen Change Loy. Fresco: Spatial-temporal correspondence for zero-shot video translation. In *Proceedings of the IEEE/CVF Conference on Computer Vision and Pattern Recognition*, pages 8703–8712, 2024. 5
- [52] Yu Zeng, Charles Ochoa, Mingyuan Zhou, Vishal M Patel, Vitor Guizilini, and Rowan McAllister. Neuralremaster: Phase-preserving diffusion for structure-aligned generation. *arXiv preprint arXiv:2512.05106*, 2025. 6
- [53] Lvmin Zhang, Anyi Rao, and Maneesh Agrawala. Adding conditional control to text-to-image diffusion models. In *Proceedings of the IEEE/CVF international conference on computer vision*, pages 3836–3847, 2023. 2, 3
- [54] Lvmin Zhang, Anyi Rao, and Maneesh Agrawala. Scaling in-the-wild training for diffusion-based illumination harmonization and editing by imposing consistent light transport. In *The Thirteenth International Conference on Learning Representations*, 2025. 3
- [55] Yabo Zhang, Yuxiang Wei, Dongsheng Jiang, Xiaopeng Zhang, Wangmeng Zuo, and Qi Tian. Controlvideo: Training-free controllable text-to-video generation 2023. URL <https://arxiv.org/abs/2305.13077>, 2023. 2
- [56] Guosheng Zhao, Xiaofeng Wang, Zheng Zhu, Xinze Chen, Guan Huang, Xiaoyi Bao, and Xingang Wang. Drivedreamer-2: Llm-enhanced world models for diverse driving video generation. In *Proceedings of the AAAI Conference on Artificial Intelligence*, pages 10412–10420, 2025. 3
- [57] Shihao Zhao, Dongdong Chen, Yen-Chun Chen, Jianmin Bao, Shaozhe Hao, Lu Yuan, and Kwan-Yee K. Wong. Uni-controlnet: All-in-one control to text-to-image diffusion models. In *Advances in Neural Information Processing Systems*, pages 1354–1367, 2023. 2
- [58] Boyang Zheng, Nanye Ma, Shengbang Tong, and Saining Xie. Diffusion transformers with representation autoencoders. *arXiv preprint arXiv:2510.11690*, 2025. 2, 3
- [59] Jun-Yan Zhu, Taesung Park, Phillip Isola, and Alexei A Efros. Unpaired image-to-image translation using cycle-consistent adversarial networks. In *Proceedings of the IEEE international conference on computer vision*, pages 2223–2232, 2017. 3



## A. Implementation details

### A.1. Training Details

We leverage the Nuplan dataset [5] to train DwD. To address the inconsistent quality of raw sequences, we implement an automated data curation pipeline utilizing Qwen3-VL [3]. This pipeline filters out samples exhibiting visual degradation—such as over-saturation, monochromatic artifacts, or other anomalies—and generates captions for the remaining data. Consequently, we compile a curated dataset of 6,000 videos, each containing 200 frames. To ensure a stable input space for DwD, we address the inherent sign ambiguity of PCA eigenvectors by establishing a consistent global feature space via Incremental PCA. Specifically, we adopt a sparse sampling strategy that extracts a single random frame from each video to compute a fixed global basis (comprising the mean and eigenvectors). This approach maximizes environmental diversity (e.g., weather conditions, time of day) while mitigating sequence-specific biases. All feature embeddings are projected onto this basis prior to training. During training, video sequences are resized to a resolution of  $1280 \times 704$  and randomly cropped into temporal chunks of 93 frames. We adopt a focused fine-tuning strategy: the parameters of the original denoising DiT are frozen, while only the copied conditional DiT is updated. Due to memory constraints (48GB VRAM), we employ Context Parallelism on a single node with 8 GPUs. The model is trained for 20k iterations with a total batch size of 1 and a learning rate of  $5 \times 10^{-5}$ .

### A.2. Data rendered from Simulator

We synthesized video sequences using the CARLA simulator across various pre-defined maps (Towns) with randomized spawn and destination points. Dynamic agents, including vehicles and pedestrians, were governed by CARLA’s built-in Traffic Manager to simulate realistic traffic flow. In total, we generated 149 videos, each averaging 200 frames. To further evaluate the generalizability of our DwD, we extended our experiments to several custom-built scenes. One visual result is illustrated in Fig. 9.

### A.3. Spatial Alignment Module and Causal Temporal Aggregator

As illustrated in Figure 6, the **Spatial Alignment Module** consists of spatial convolutions and residual blocks. When integrating the **Causal Temporal Aggregator**, we prefix the input DINO latent sequence with zero-padding to ensure the temporal convolutions maintain causality.

## B. Qualitative Comparisons across Ablated Hyperparameters

In this section, we provide extensive visual comparisons to substantiate the quantitative observations discussed in the

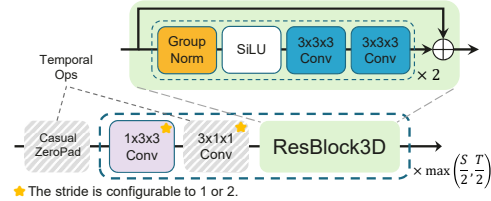


Figure 6. The Spatial Alignment Module and Causal Temporal Aggregator.

main paper. specifically, we examine the impact of key hyperparameters and architectural choices on the visual quality, structural fidelity, and temporal consistency of the generated videos.



Figure 7. Qualitative Comparison across Minor Components Pruning Degree ( $k$ )

### B.1. Analysis of Naive DINO Latent Injection

As hypothesized in the main methodology, directly utilizing non-pruned DINO latents as the control signal introduces significant information redundancy. We visualize this phenomenon in the first row of Fig. 7. Compared to DwD, the naive implementation exhibits severe **texture leakage**, where the high-frequency surface details of the source CG

input (e.g., wireframes or flat shading artifacts) are inadvertently preserved in the generated output. This leakage prevents the generative model from effectively synthesizing new textures, resulting in a video that appears merely as a filtered version of the input rather than a semantically consistent regeneration. In contrast, DwD successfully disentangles structure from texture, preserving the geometric layout while allowing for realistic rendering.

## B.2. Impact of Minor Components Pruning Degree ( $k'$ )

The pruning of minor components, modulated by the PCA clamping factor  $k'$ , functions as a critical regularizer within the information bottleneck framework. As illustrated in Fig. 7, this parameter regulates the trade-off between structural guidance and generative flexibility:

- **Insufficient Pruning ( $k' = 32$ ):** A larger  $k$  preserves excessive trivial feature variance. Consistent with the quantitative results in the main paper, this results in a degradation of realism, as the model becomes over-constrained by noise and irrelevant artifacts inherited from the source domain.
- **Excessive Pruning ( $k' = 3$ ):** Conversely, overly aggressive pruning compromises the semantic integrity of the scene. At  $k = 3$ , the control signal becomes too sparse to accurately encapsulate complex geometries, leading to structural hallucinations where the generated content deviates from the layout of the input CG scene. For instance, as shown in Fig. 7 (Row 5), a bridge is erroneously synthesized in the distant background. Furthermore, this configuration undermines a key advantage of DwD: its robustness against degradation during autoregressive long-



Figure 8. Qualitative Comparison across different Upscaling Factors  $\times S$  in *Spatial Resolution Enhancement*. The **red boxes** highlight inconsistencies with respect to the CG input.

video generation, which will be discussed subsequently.

## B.3. Effect of Spatial Upscaling Factor ( $S$ )

We further investigate the upscaling factor  $S$  of *Spatial Resolution Enhancement*. Visual results in Fig. 8 indicate a positive correlation between the spatial upscaling factor  $S$  and structural consistency.  $S = 4$  provide fine-grained geometric cues, enabling the model to align generated instances more precisely with the input. Lower resolutions ( $S = 1$ ) tend to produce incorrect stuffs, like translating street lamps into traffic light.

## B.4. Efficacy of the Causal Temporal Aggregator

Finally, we evaluate the contribution of the *Causal Temporal Aggregator* by comparing it with a naive and popular key-frame sampling strategy. As illustrated in Fig. 10, under fast camera jittering, The naive approach leads to observable motion blurs and discontinuities. In contrast, our Temporal Aggregator effectively smooths the transitions across frames. The visual comparison highlights that our module significantly mitigates **motion blur** and flickering artifacts, yielding video sequences with superior temporal coherence and stability.

## C. Upsampling using Anyup

While feature upsampling methods such as AnyUp [46] appear to offer a computationally efficient alternative for obtaining high-resolution DINO feature maps, we empirically find that they consistently lead to unstable controllability in video generation, resulting in the suboptimal quantitative metrics and poor visual quality. To investigate this, we visualize the PCA components of feature maps upsampled via AnyUp versus naive input upscaling in Fig. 11. We observe that since AnyUp incorporates high-resolution RGB images as guidance, it inadvertently introduces unnecessary high-frequency pixel information, leading to feature quality degradation. As highlighted by the red boxes, the pixel-level guidance causes AnyUp to misinterpret texture differences (e.g., between the curb and the neighboring ground) as distinct semantic categories, whereas naive upscaling maintains a more coherent semantic representation. Furthermore, as shown in the green boxes, AnyUp fails to recover fine-grained structural details despite an  $8\times$  upsampling factor; for instance, the boundaries between distant street lamps and the sky remain indistinct. These visual observations corroborate our experimental findings, confirming that the feature degradation inherent in AnyUp is the primary cause of the generation instability.

## D. Robust Long Video Generation using DwD

A distinctive advantage of DwD is its superior robustness in autoregressive long-horizon driving video generation.



Frame 0 → Frame 622



Figure 9. Qualitative comparison of autoregressive long video generation.





Figure 10. Qualitative Comparison w. and w./o. *Causal Temporal Aggregator*

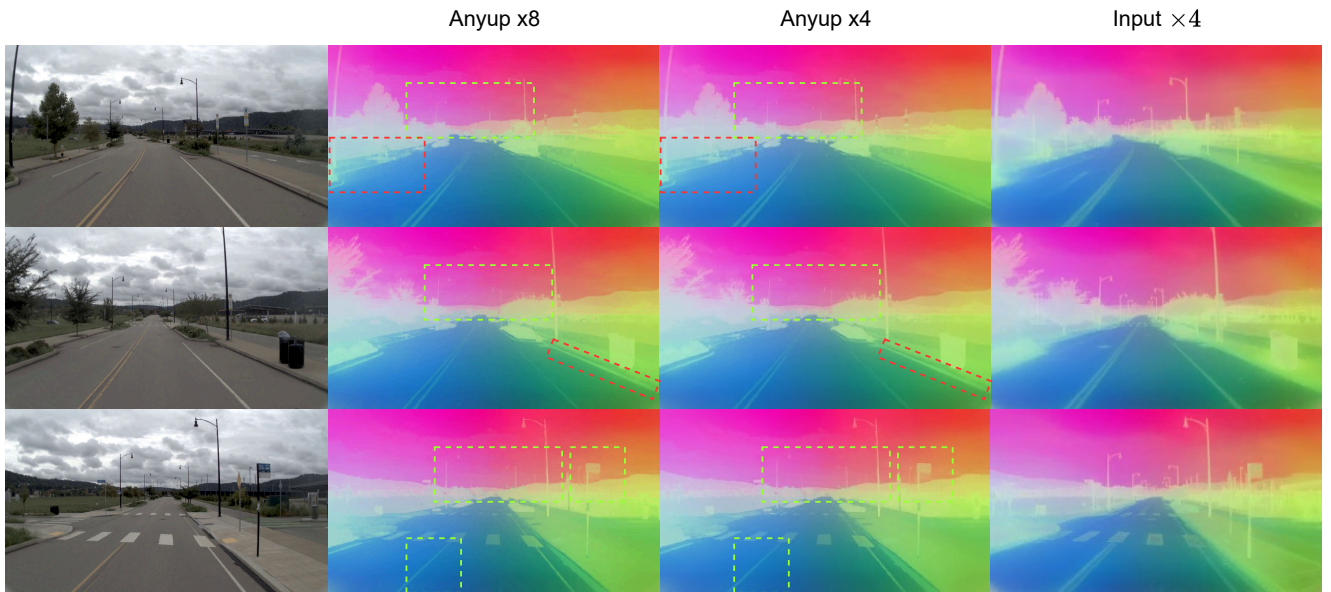


Figure 11. PCA visualization comparing feature maps upsampled via AnyUp ( $\times 4$  and  $\times 8$ ) versus naive input upscaling ( $\times 4$ ). The **red boxes** highlight semantic inconsistencies introduced by AnyUp, where high-frequency pixel information leads to false semantic boundaries (e.g., misclassifying the curb). The **green boxes** demonstrate the failure of AnyUp to recover fine-grained structural details, such as the boundaries of distant street lamps, despite the high upsampling factor.

Leveraging the Cosmos Predict 2.5 backbone with a 93-frame chunk size, we observe that most Cosmos Transfer 2.5 control branches suffer from severe error accumulation and degradation after approximately three generation cycles. In contrast, our method effectively maintains visual fidelity, avoiding common artifacts such as color oversaturation. Qualitative comparisons are illustrated in Fig. 9; we explicitly recommend reviewing the supplementary videos for a dynamic evaluation of temporal consistency.

## E. Extra Qualitative Comparisons

Figure 12. **Extra Qualitative comparison with state-of-the-art methods.** The **red boxes** highlight **inconsistencies** with respect to the CG input, while the **green boxes** point out **low-fidelity textures**.

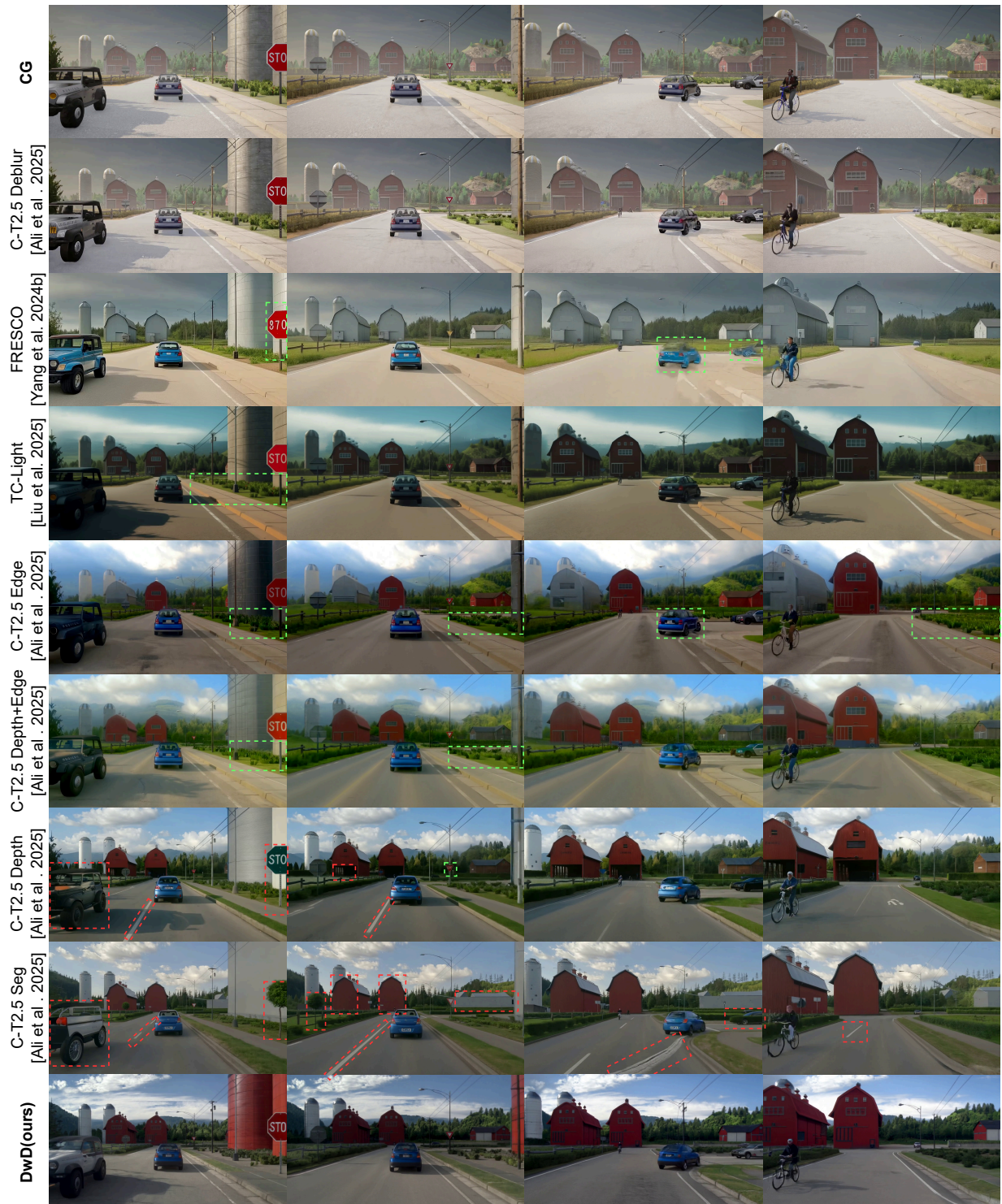




Figure 13. **Extra Qualitative comparison with state-of-the-art methods.** The **red boxes** highlight **inconsistencies** with respect to the CG input, while the **green boxes** point out **low-fidelity textures**.

